DRUG DELIVERY
2022, VOL. 29, NO. 1, 263–269
https://doi.org/10.1080/10717544.2021.2023695

Taylor & Francis
Taylor & Francis Group

RESEARCH ARTICLE

OPEN ACCESS Check for updates

Combination anesthetic therapy: co-delivery of ropivacaine and meloxicam using transcriptional transactivator peptide modified nanostructured lipid carriers *in vitro* and *in vivo*

Shu Yuan[a], Jun Chen[a], Shuo Feng[b], Min Li[a], Yingui Sun[a] and Yuzhen Liu[b]

[a]Department of Anesthesiology, Weifang Medical University, Weifang, China; [b]Department of Gynecology, Affiliated Hospital of Weifang Medical University, Weifang, China

ABSTRACT

Combination therapy combining two drugs in one modified drug delivery system is used to achieve synergistic analgesic effect, and bring effective control of pain management, especially postoperative pain management. In the present study, a combination of drug delivery technologies was utilized. Transcriptional transactivator (TAT) peptide modified, transdermal nanocarriers were designed to co-deliver ropivacaine (RVC) and meloxicam (MLX) and anticipated to achieve longer analgesic effect and lower side effect. TAT modified nanostructured lipid carriers (TAT-NLCs) were used to co-deliver RVC and MLX. RVC and MLX co-loaded TAT-NLCs (TAT-NLCs-RVC/MLX) were evaluated through *in vitro* skin permeation and *in vivo* treatment studies. NLCs-RVC/MLX showed uniform and spherical morphology, with a size of 133.4 ± 4.6 nm and a zeta potential of 20.6 ± 1.8 mV. The results illustrated the anesthetic pain relief ability of the present constructed system was significantly improved by the TAT modification through the enhanced skin permeation efficiency and the co-delivery of MLX along with RVC that improved pain management by reducing inflammation at the injured area. This study provides an efficient and facile method for preparing TAT-NLCs-RVC/MLX as a promising system to achieve synergistic analgesic effect.

ARTICLE HISTORY
Received 27 September 2021
Revised 16 December 2021
Accepted 20 December 2021

KEYWORDS
Combination anesthetic; co-delivery; ropivacaine; meloxicam; nanostructured lipid carriers

Introduction

Effective control of pain management, especially postoperative pain management, remains challenging up to now (Mathiesen et al., 2012; Rawal, 2016). Researchers have estimated that 75% surgical patients did not accept adequate pain relief in the USA, and their pain converted from acute postoperative pain (nociceptive and inflammatory pain) to chronic pain (Kehlet et al., 2006; Wu & Raja, 2011; Gan et al., 2014; Ji et al., 2016). Therefore, there is a compelling need for exploiting novel drug delivery system and drug combination therapy.

Common drugs widely used for postoperative analgesia include opioids, and nonopioids such as local anesthetics (LAs) and nonsteroidal anti-inflammatory drugs (NSAIDs) (Brigham et al., 2021). Due to opioid-related adverse events (respiratory depression, nausea, vomiting, etc.) and short analgesic time (12–24 h) from common LAs injection, various researchers have dedicated themselves to more effective non-opioid analgesics (72 h or more analgesic time), and two new formulations have been approved by the FDA that are liposomal bupivacaine EXPAREL (via injection into the surgical site), and bupivacaine/meloxicam (MLX) extended release solution ZYNRELEF KIT (via instillation into the surgical site) (Balocco et al., 2018; Shah et al., 2018; Prabhakar et al., 2019; Ottoboni et al., 2020). LAs (bupivacaine, etc.) and NSAIDs (meloxicam, etc.) combination therapy combine with two different mechanisms of action to achieve synergistic analgesic effect, and bring new era in the clinical area of analgesia (Viscusi et al., 2019). In the present study, transdermal nanocarriers were designed to co-deliver ropivacaine (RVC) and MLX and anticipated to achieve longer analgesic effect and lower side effect.

Ropivacaine, a new aminoamide LA, shows longer analgesic duration (up to 12 h) and less cardiovascular or central nervous system toxicities compared with bupivacaine (Scott et al., 1989; Yang et al., 2019). Ropivacaine hydrochloride injection (Naropin) has been approved for local or regional anesthesia of surgery and for acute pain management, with a plasma clearance rate of 8 L/min, a renal clearance rate of 1 mL/min, and a final half-life of 1.8 h (Peskin, 2005). Due to its appropriate physicochemical property (log $P = 2.9$, low molecule weight = 274.41), the prerequisites for transdermal delivery system are met (McClure, 1996).

Meloxicam, a long-acting NSAID, inhibits cyclooxygenase-2 (COX-2, highly inducible after tissue injury and inflammation) over cyclooxygenase-1 (COX-1) that can alleviate pain and reduce inflammation at the injured area (Samad et al., 2001). Meloxicam injection (ANJESO) has been approved for use in adults for the management of moderate-to-severe

CONTACT Yingui Sun yinguisunsdpc@163.com; Yuzhen Liu yuzhenliuwmu@hotmail.com No. 7166 Baotong West Street, Weifang 261053, Shandong Province, China

pain, alone or in combination with non-NSAID analgesics, with a time to peak of 0.12 h and a half-life period of 23.3 h (Anjeso, 2020). Due to its poor aqueous solubility and low skin permeation, researchers have designed suitable transdermal drug delivery system (nanostructured lipid carriers, NLCs) for MLX delivery (Khalil et al., 2014; Khurana et al., 2015).

Current postoperative pharmacotherapy is typically achieved by injectable, transdermal, or subcutaneous routes (Brigham et al., 2021). Transdermal drug delivery system is an effective method for achieving localized drug delivery that can alleviate anxiety and discomfort caused by needle insertion, especially relive pain for up to 3 h or 3 months via self-administered by the patient (de Araújo et al., 2013; You et al., 2017).

In the previous study, a transcriptional transactivator peptide (TAT) modified lidocaine loaded nanostructured lipid carriers (NLCs) was designed for topical anesthetic therapy (Wang et al., 2016). In the present study, TAT modified NLCs (TAT-NLCs) were used to co-deliver RVC and MLX. RVC and MLX co-loaded TAT-NLCs (TAT-NLCs-RVC/MLX) were evaluated through *in vitro* skin permeation and *in vivo* treatment studies.

Materials and methods

Materials

Transcriptional transactivator peptide–polyethylene glycol$_{2000}$–distearoyl phosphoethanolamine (TAT–PEG$_{2000}$–DSPE) was prepared by our lab as reported before (Wang et al., 2016). Ropivacaine, meloxicam,Tween-80, and stearic acid were purchased from Sigma Aldrich (St. Louis, MO). Polyoxyl castor oil (Cremophor ELP) was donated by BASF (Ludwigshafen, Germany); soybean phospholipids (SPCs) were purchased from Taiwei Pharmaceuticals (Shanghai, China); Labrafac PG (propylene glycol dicaprylocaprate) was a kind offer from Gattefossé (Gennevilliers, France). All other reagents and solvents were analytical or high-performance liquid chromatography (HPLC) grade. Kunming mice (4–6 weeks old, 18–22 g weight) were purchased from the Medical Animal Test Center of Shandong University. The animal experiments followed the guidance of the National Institutes of Health (NIH) for the care and use of laboratory animals.

Preparation of TAT-NLCs

TAT-NLCs were prepared by emulsion evaporation–solidification method (Wang et al., 2016). Briefly, SPC (20 mg), Labrafac PG (20 mg), and Cremophor ELP (1 mL) were dissolved in 9 mL ethanol at 60 °C to get the oil phase. TAT–PEG$_{2000}$–DSPE (100 mg) and Tween-80 (1%) were dissolved in 40 mL double distilled water to form an aqueous phase. The oil phase was then added dropwise into the aqueous phase and the whole system was kept stirring (400 r/min) by a C-MAG HS 10 digital magnetic stirrer (IKA-Labortechnik, Staufen, Germany) in 60 °C for 3 h in order to remove the organic solvents. Then, the nanoemulsion was added into 50 mL of distilled water at 0 °C immediately and stirred for 30 min. TAT-NLCs were harvested and stored at 2–8 °C (method 1). The amount of SPC, Labrafac PG, Cremophor ELP, TAT–PEG$_{2000}$–DSPE, and Tween-80 used was screened by single factor and orthogonal design.

TAT-NLCs-RVC/MLX (Figure 1) were prepared similar to the method 1 above: the aqueous phase was the same; the oil phase was prepared using RVC (2 mg), MLX (2 mg), SPC (20 mg), Labrafac PG (20 mg), and Cremophor ELP (1 mL) dissolved in 9 mL ethanol.

RVC loaded TAT-NLCs (TAT-NLCs-RVC) were prepared similar to the method 1 above: the aqueous phase was the same; the oil phase was prepared using RVC (2 mg), SPC (20 mg), Labrafac PG (20 mg), and Cremophor ELP (1 mL) dissolved in 9 mL ethanol.

MLX loaded TAT-NLCs (TAT-NLCs-MLX) were prepared similar to the 'method 1' above: the aqueous phase was the same; the oil phase was prepared using MLX (2 mg), SPC (20 mg), Labrafac PG (20 mg), and Cremophor ELP (1 mL) dissolved in 9 mL ethanol.

RVC and MLX co-loaded NLCs which were not modified by TAT ligands (NLCs-RVC/MLX) were prepared using 'method 1' above: the oil phase was the same; the aqueous phase was prepared using Tween-80 (1%) dissolved in 40 mL double distilled water.

Characterization of NLCs

The particle size, polydispersity index (PDI), and zeta potential of NLCs were measured using Zetasizer Nano (Malvern Instruments, Malvern, UK) (Hong et al., 2019). The morphology and size of TAT-NLCs-RVC/MLX imaged by a transmission electron microscope (TEM, JEOL Ltd., Tokyo, Japan). Drug encapsulation efficiency (EE) and drug loading (DL) capacity were evaluated by quantifying the amount of RVC and MLX loaded in the NLCs. The amount of entrapped RVC was detected by reverse-phase HPLC using an Agilent 1200 system equipped with a UV monitor (Agilent G1314-60100, Santa Clara, CA) (Zhai et al., 2015). Separations were carried out using a BDS C18 column (250 × 4.6 mm, 5 μm). RPV was detected at 225 nm with a mobile phase containing a mixture of acetonitrile:phosphate buffer (60:40) at a flow-rate of 1.0 mL/min. The amount of MLX was analyzed at 360 nm using validated UV-spectrophotometric method (Shimadzu, Kyoto, Japan) (Khalil et al., 2014). The EE and DL were calculated as follows:

$$\text{EE}\ (\%) = \text{amount of drugs loaded in the NLCs} / \text{amount of fed drugs} \times 100;$$

$$\text{DL}\ (\%) = \text{amount of drugs loaded in the NLCs} / \text{all materials in the system} \times 100.$$

Stability of NLCs

Stability of NLCs was evaluated by observing the appearance, diameter, and EE of the systems during the storage time at

the temperature of 30 ± 2 °C and 2–8 °C (Chen & You, 2017). The results were calculated and then analyzed at the predetermined time intervals (0, 30, 60, and 90 days).

In vitro *cytotoxicity of NLCs*

The cytotoxicity of NLCs was evaluated by CCK-8 assay (Zhang et al., 2017). L929 cells were seeded into 96-well plates (5×10^4 cells/well) and incubated for 24 h. Drugs loaded NLCs and free drugs (drugs in 1.5% Carbomer 940 to form gels) were added to the cells and incubated for another 48 h, then CCK-8 solution (10 μL) was added to each well and cells were incubated for 1 h. Absorbance at 450 nm was measured and cell viability (CV) as calculated as follows:

$$\mathrm{CV}\ (\%) = \text{absorbance of cells treated with samples} / \text{absorbance of cells treated with fresh medium} \times 100.$$

In vitro *skin permeation efficiency of NLCs*

In vitro skin permeation efficiency of NLCs was evaluated using the abdominal full-thickness skins of SD rats (Yang et al., 2019). Briefly, SD rats were sacrificed and the fur on the abdominal area of the rats was removed and the adherent muscle, fat, vasculature, and subcutaneous tissue were excised. The stripped skin was tied between the donor and receptor compartment of the Franz diffusion cells with an effective permeation area of 3.14 cm^2. The receptor compartment was filled with PBS (pH 7.4) under constantly stirring (400 rpm). Drugs loaded NLCs and drugs solution (0.5 mL, 5 mg/mL) were added to the skin and samples (0.3 mL) were collected from the receptor compartment, then equivalent amount of PBS was added. The amount of permeated drugs was analyzed by HPLC and the cumulative amount of drugs penetrated (P_n) was calculated using equation: $P_n = \left(C_n \times V_0 + \sum_{i=0}^{n-1} C_i \times V_i\right)/A$, where C_n and C_i refer to the drug concentration of the receptor medium at each sampling time and the drug concentration of the *i*th sample, respectively; V_0 and V_i correspond to the volumes of the receptor compartment and the collected sample, respectively; A means the effective diffusion area. The steady-state fluxes (J_{ss}) were obtained by representing the amount of drug permeated per unit area versus time. The permeability coefficient (K_p) was calculated using the equation: $K_p = J_{ss}/C_0$, where C_0 corresponds to the drug concentration in the donor compartment.

In vivo *skin permeation ability of NLCs*

In vivo skin permeation ability of NLCs was evaluated on the abdominal site of SD rats (Liu & Zhao, 2019). The hair at the abdominal site of rats was shaved off and the skin area was washed with distilled water. Drugs loaded NLCs and drugs solution (0.5 mL, 5 mg/mL) were applied on the skin surface (4 cm^2) then bound with gauze. At predetermined time points, rats were sacrificed and the skin was cut into pieces, homogenized with methanol and acetonitrile. The mixture was then separated by centrifuging (12,000 rpm, 10 min) and the amount of drugs was analyzed by HPLC as described in 'Characterization of NLCs' section.

In vivo *anesthetic pain relief assessment*

The plantar surface of the left hind paw of each rat was prepared aseptically, and the incisional pain model was created by making a longitudinal skin incision (1 cm) extending toward the digits with a blade at a point approximately 0.5 cm distal to the tibiotarsal joint on the plantar surface of the left hind paw (Choi et al., 2020). For testing mechanical allodynia, the rats were placed in a testing chamber and permitted to acclimatize for 30 min prior to testing. Von Frey filaments with scores of 2, 4, 6, 8, 10, 15, 26, and 60 g were applied to the soft tissue of the left hind paw to determine withdrawal thresholds (Safakhah et al., 2016). The force applied by the first filament is equivalent to 2 g. Apply each filament three times, each time three seconds followed by five seconds intervals. If a negative reaction was seen (no movement), the filament applies the next greater force. If the two responses observed were positive (paw retraction), the score obtained was considered to be a response threshold. If the animal did not respond to a 60 g score, that score was considered a threshold response.

Statistical analysis

Results are presented as means ± standard deviation (SD). Statistical analyses were performed using Student's *t*-test and a value of $p < .05$ was considered statistically significant.

Results

Characterization of NLCs

TAT-NLCs-RVC/MLX showed uniform and spherical morphology (Figure 1) with a size of 133.4 ± 4.6 nm (Table 1), which is larger than that of NLCs-RVC/MLX (101.9 ± 4.2 nm). The zeta potential of TAT-NLCs-RVC/MLX and NLCs-RVC/MLX was 20.6 ± 1.8 and 10.3 ± 1.3 mV, respectively. All the TAT-NLCs showed similar size and surface change. The EE of NLCs was around 90%. During 90 days of storage time at the temperature of 2–8 °C, the appearance, diameter, and EE of NLCs were not changed (data not shown), proving the stability of the systems. The diameter and EE of NLCs remained unchanged for 96 hours under the condition of 30 ± 2 °C.

In vitro *cytotoxicity*

In vitro cytotoxicity of drugs loaded NLCs and free drugs was evaluated by the L929 cells viability (Figure 2). Drugs loaded NLCs showed negligible cytotoxicity on cells at the study concentrations, while free drugs showed cell inhibition effects on cells at the higher concentrations (from 20 to 100 μM).

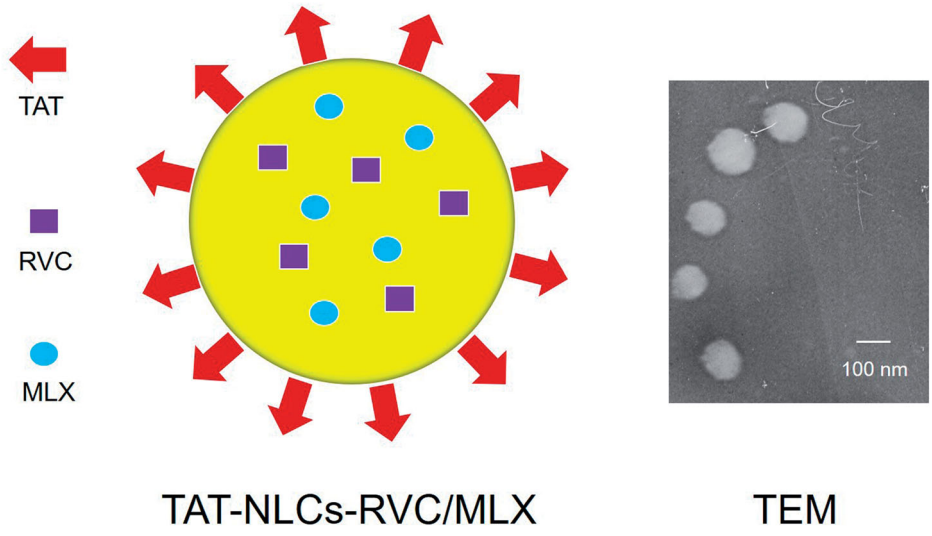

Figure 1. Scheme graph and morphology of TAT-NLCs-RVC/MLX.

Table 1. Characterization of NLCs (mean ± SD, $n = 3$).

				EE (%)		DL (%)	
Formulation	Particle size (nm)	PDI	Zeta potential (mV)	RVC	MLX	RVC	MLX
TAT-NLCs	131.5 ± 5.1	0.16 ± 0.02	22.1 ± 1.9	–	–	–	–
TAT-NLCs-RVC/MLX	133.4 ± 4.6	0.14 ± 0.02	20.6 ± 1.8	93.5 ± 3.1	89.9 ± 3.2	10.3 ± 0.9	9.5 ± 0.7
TAT-NLCs-RVC	134.1 ± 4.3	0.13 ± 0.01	21.5 ± 1.6	91.7 ± 2.9	–	11.1 ± 0.7	–
TAT-NLCs-MLX	129.8 ± 4.8	0.17 ± 0.02	19.8 ± 2.1	–	90.8 ± 3.2	–	10.1 ± 0.8
NLCs-RVC/MLX	101.9 ± 4.2	0.15 ± 0.02	10.3 ± 1.3	90.8 ± 2.7	91.3 ± 2.9	12.2 ± 1.1	13.1 ± 0.9

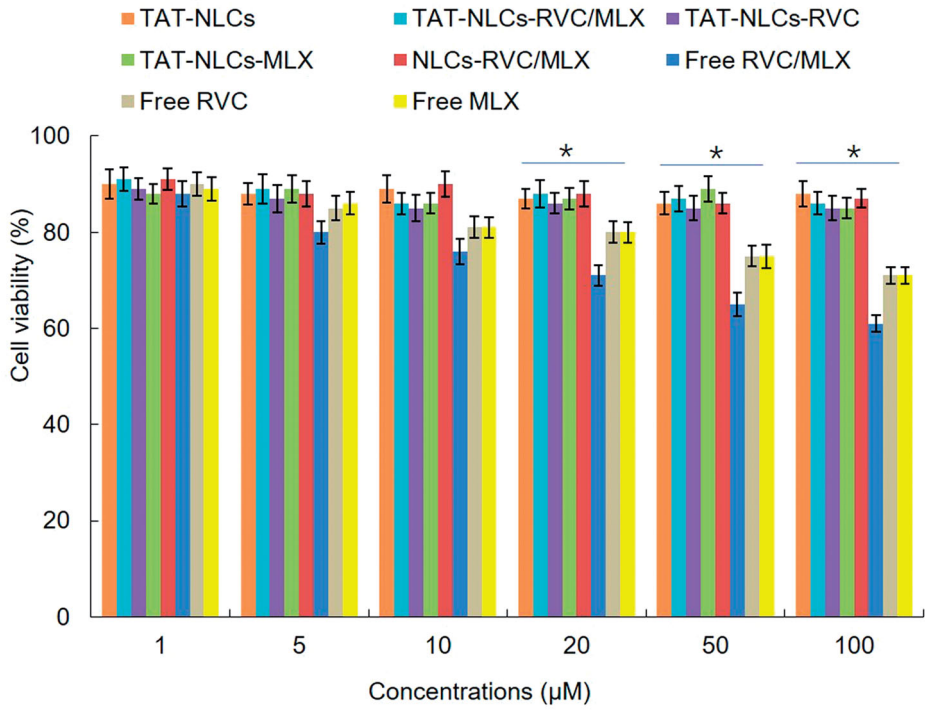

Figure 2. *In vitro* cytotoxicity of drugs loaded NLCs and free drugs evaluated by the L929 cells viability. Data presented as means ± SD ($n = 3$). *$p < .05$.

In vitro *skin permeation efficiency*

In vitro skin permeation efficiency of drugs from NLCs and free drugs was compared using the Franz diffusion cells with the skin of rats (Figure 3). Figure 3(A,B) illustrates the accumulative penetration curves of RVC and MLX, and the penetration parameters are summarized in Table 2. The data showed that TAT-NLCs significantly improved the permeation efficiency of drugs when compared with unmodified NLCs, the latter also exhibited better skin permeation ability than that of free drugs ($p < .05$). After 48 h of drug administration,

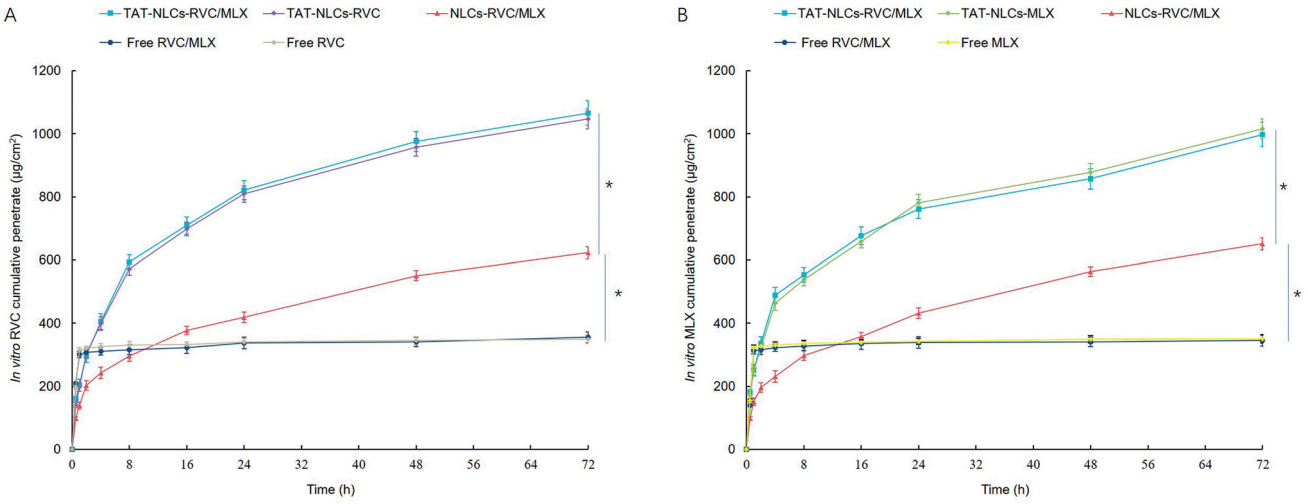

Figure 3. *In vitro* skin permeation efficiency of RVC (A) and MLX (B) from NLCs and free drugs compared using the Franz diffusion cells with the skin of rats. Data presented as means ± SD ($n = 3$). *$p < .05$.

Table 2. Permeation parameters of RVC from NLCs and solution (mean ± SD, n = 3).

Formulations	P_{48} (μg·cm^{-2})	J_{ss} (μg·cm^{-2}·h^{-1})	K_p (cm·h^{-1})
TAT-NLCs-RVC/MLX	898.3 ± 28.9	12.3	6.5×10^{-3}
TAT-NLCs-RVC	903.4 ± 22.6	12.9	6.8×10^{-3}
NLCs-RVC/MLX	513.7 ± 20.9	7.1	3.7×10^{-3}
Free RVC/MLX	312.6 ± 15.5	4.8	2.5×10^{-3}
Free RVC	308.7 ± 19.1	4.6	2.4×10^{-3}

the RVC permeation amount of TAT-NLCs-RVC/MLX, NLCs-RVC/MLX, and free RVC/MLX was 898.3 ± 28.9, 513.7 ± 20.9, and 312.6 ± 15.5 μg·cm^{-2}, respectively (Table 2). TAT-NLCs-RVC/MLX exhibited the most prominent permeability coefficient (K_p), which is 2.6-fold compared with free RVC/MLX.

In vitro *skin permeation ability*

In vivo skin permeation profiles of drugs from NLCs and free drugs (Figure 4) were different from *in vitro* permeation results. Fewer drugs were penetrated through the skin from free drugs groups compared with *in vitro* study. TAT-NLCs-RVC/MLX exhibited enhanced *in vivo* drugs penetration ability, better than that of NLCs-RVC/MLX and free RVC/MLX. Comparing Figure 4 with Figure 3, conclusion could be made that at the first 1 h, free drugs showed well permeation efficiency *in vitro* while the *in vivo* permeation ability was not ideal. However, the permeation behaviors of NLCs formulations were similar, which could be the evidence of the NLCs formulations could improve the *in vivo* efficiency of drugs.

In vivo *anesthetic pain relief efficacy*

In vivo anesthetic pain relief effects of drugs loaded NLCs and free drugs are presented in Figure 5. We can tell that all the drugs contained formulas that exhibited anesthetic pain relief ability to some extent. Free drugs formulations showed a rapid but short-lasting anesthetic effect, with a peak effect seen within the first 1 or 2 h after drug application. However, NLCs formulation increased the pain relief time, the effects last for 72 h. The strongest anesthetic pain relief was achieved by TAT-NLCs-RVC/MLX, which showed a peak value of 53.3 ± 3.1 g. These data were better than that of single RVC-loaded TAT-NLCs-RVC and unmodified NLCs-RVC/MLX ($p < .05$).

Discussion

In the present study, TAT-NLCs were used to co-deliver RVC and MLX. We have compared the use of SPCs with egg yolk lecithin; use of Labrafac PG, Cremophor ELP, and Capryol90. After comparison, the types and amount of lipid in the preparation of NLCs were selected. TAT-NLCs-RVC/MLX showed uniform and spherical morphology, with a size of 133.4 ± 4.6 nm and a zeta potential of 20.6 ± 1.8 mV. As Zhang et al. discussed that the small particle size of the delivery system may enhance the bioavailability of bioactive compounds, adhesion efficiency with biological cells, thus resulting in an occlusive effect on the skin layer could lead to a long duration of action of the drug (Zhang et al., 2016). The appearance and diameter of NLCs were not changed during 90 days of storage time, proving the stability of the systems. Zhang et al. reported that the storage stability of nanoparticles coud be evaluated by measuring the average particle diameter of nanoparticles throughout the storage period, which could be the evidence that no aggregate was observed (Zhang et al., 2018). In our study, we also add the appearance into this section thus can further determine the stability of the systems.

Evaluation of the cytotoxicity of the nanoparticles is essential, because we need to exclude the materials that used which may bring about cytotoxic effects (Lee et al., 2015). *In vitro* cytotoxicity of RPV-LPNs and E-LPNs is negligible at all the studied concentrations, which may be used as safety *in vivo*. The drugs loaded NLCs constructed in this study showed negligible cytotoxicity on cells at the study concentrations, proving the low toxicity of the nano-systems.

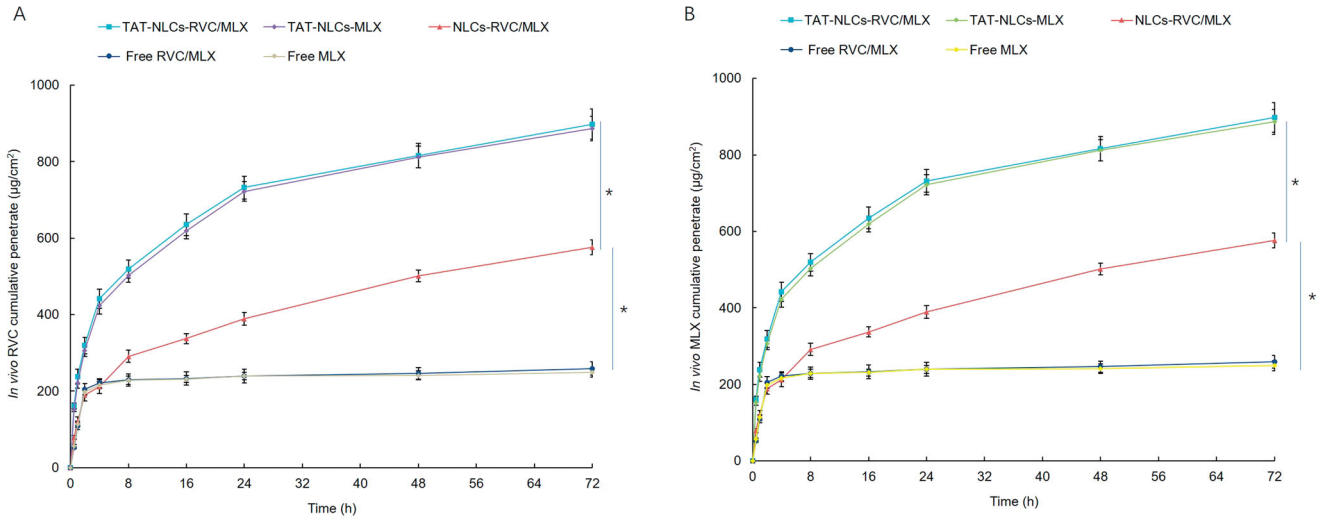

Figure 4. *In vivo* skin permeation profiles of RVC (A) and MLX (B) from NLCs and free drugs evaluated on the abdominal site of SD rats. Data presented as means ± SD ($n = 3$). *$p < .05$.

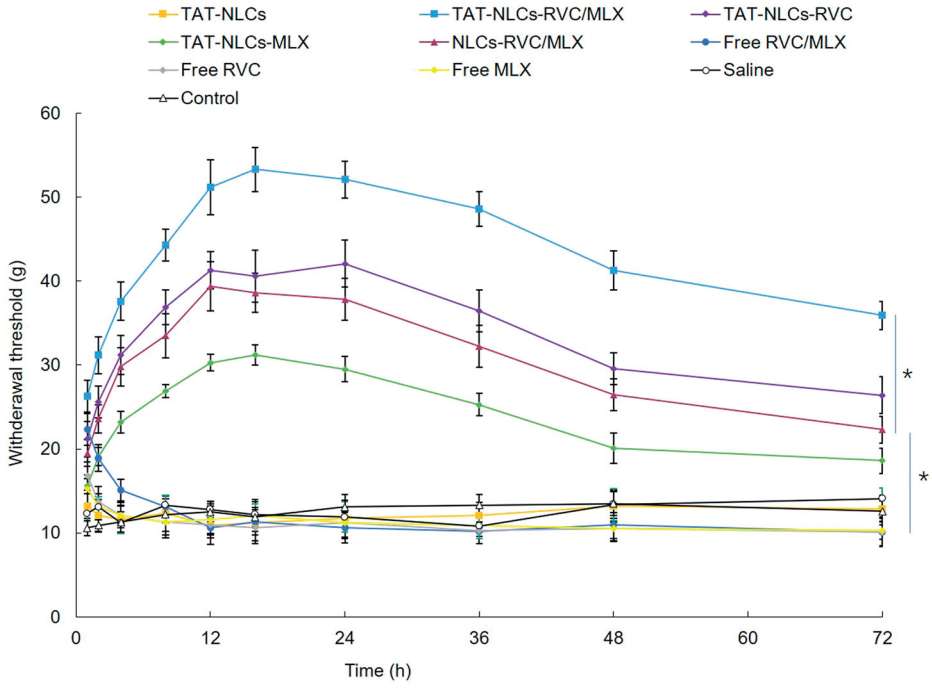

Figure 5. *In vivo* anesthetic pain relief effects of drugs loaded NLCs and free drugs. Data presented as means ± SD ($n = 3$). *$p < .05$.

Li et al. argue that if nano-systems showed negligible cytotoxicity *in vitro*, they may be used as safety *in vivo* (Li et al., 2019).

In vitro and *in vivo* skin permeation efficiency of NLCs was evaluated using the abdominal full-thickness skins of SD rats and on the abdominal site of SD rats, respectively. Shah et al. informed that TAT is known to have higher permeation enhancing ability which is mainly because of the presence of cationic amino acids like arginines and lysines (Shah et al., 2012). TAT contained more than six arginine groups which might result in enhanced permeation and thus improved skin permeation. In this study, TAT-NLCs-RVC/MLX exhibited better skin permeation ability compared with unmodified NLCs-RVC/MLX both *in vitro* and *in vivo*. These results were in accordance with the founding of Chen and You, who said that after TAT decoration was accomplished, its penetration rate and flux were significantly higher than non-decorated nano-systems (Chen & You, 2017). Yue et al. summarized that due to the lipid-rich environment of the stratum corneum, lipophilic molecules of NLCs are well suited for translocation across corneum. NLCs have a natural affinity for skin lipids, which allows them to facilitate drug transport by favoring the partitioning of the drug from the vehicle into the skin (Yue et al., 2018). In this research, NLCs formulations significantly improved the drug efficiency, which reflected in the improved skin permeation efficiency than that of free drug formulations.

In vivo anesthetic pain relief effects were assessed in rats whose left hind paw were injured. Meloxicam is a

long-acting NSAID, which can alleviate pain and reduce inflammation at the injured area (Samad et al., 2001). Since MLX has anti-inflammatory activities, it may be useful in reducing the resulting pain behaviors in the prepared rats (Khalil et al., 2014). In the present research, TAT-NLCs-RVC/MLX showed better anesthetic pain relief ability than that of single RVC loaded TAT-NLCs-RVC, which could prove the reduction effect of MLX that enhanced the efficiency of the whole system. These results illustrated the anesthetic pain relief ability of the present constructed system was significantly improved by the TAT modification through the enhanced skin permeation efficiency and the co-delivery of MLX along with RVC that improved pain management by reducing inflammation at the injured area. TAT-NLCs-RVC/MLX could be used as a promising system to achieve synergistic analgesic effect.

Disclosure statement

No potential conflict of interest was reported by the author(s).

Funding

This study was supported by Shandong Medical Association Comfort-Anesthesia Optimization Special Project (2021 No. YXH2021ZX027). Shandong Medicine and Health Science and Technology Development Project (No. 202104110339; No.2019WS605).

References

Balocco AL, Van Zundert PGE, Gan SS, et al. (2018). Extended release bupivacaine formulations for postoperative analgesia: an update. Curr Opin Anaesthesiol 31:636–42.

Brigham NC, Ji RR, Becker ML. (2021). Degradable polymeric vehicles for postoperative pain management. Nat Commun 12:1367.

Chen C, You P. (2017). A novel local anesthetic system: transcriptional transactivator peptide-decorated nanocarriers for skin delivery of ropivacaine. Drug Des Devel Ther 11:1941–9.

Choi GJ, Kang H, Lee JM, et al. (2020). Effect of intraperitoneally administered propentofylline in a rat model of postoperative pain. Korean J Pain 33:326–34.

de Araújo DR, da Silva DC, Barbosa RM, et al. (2013). Strategies for delivering local anesthetics to the skin: focus on liposomes, solid lipid nanoparticles, hydrogels and patches. Expert Opin Drug Deliv 10:1551–63.

Gan TJ, Habib AS, Miller TE, et al. (2014). Incidence, patient satisfaction, and perceptions of post-surgical pain: results from a US National Survey. Curr Med Res Opin 30:149–60.

Hong Y, Che S, Hui B, et al. (2019). Lung cancer therapy using doxorubicin and curcumin combination: targeted prodrug based, pH sensitive nanomedicine. Biomed Pharmacother 112:108614.

Anjeso. (2020). IV meloxicam (Anjeso) for pain. Med Lett Drugs Ther 62:100–2.

Ji RR, Chamessian A, Zhang YQ. (2016). Pain regulation by non-neuronal cells and inflammation. Science 354:572–7.

Kehlet H, Jensen TS, Woolf CJ. (2006). Persistent postsurgical pain: risk factors and prevention. Lancet 367:1618–25.

Khalil RM, Abd-Elbary A, Kassem MA, et al. (2014). Nanostructured lipid carriers (NLCs) versus solid lipid nanoparticles (SLNs) for topical delivery of meloxicam. Pharm Dev Technol 19:304–14.

Khurana S, Jain NK, Bedi PM. (2015). Nanostructured lipid carriers based nanogel for meloxicam delivery: mechanistic, in-vivo and stability evaluation. Drug Dev Ind Pharm 41:1368–75.

Lee YK, Choi EJ, Webster TJ, et al. (2015). Effect of the protein corona on nanoparticles for modulating cytotoxicity and immunotoxicity. Int J Nanomedicine 10:97–113.

Li A, Yang F, Xin J, Bai X. (2019). An efficient and long-acting local anesthetic: ropivacaine-loaded lipid–polymer hybrid nanoparticles for the control of pain. Int J Nanomedicine 14:913–20.

Liu X, Zhao Q. (2019). Long-term anesthetic analgesic effects: comparison of tetracaine loaded polymeric nanoparticles, solid lipid nanoparticles, and nanostructured lipid carriers in vitro and in vivo. Biomed Pharmacother 117:109057.

Mathiesen O, Thomsen BA, Kitter B, et al. (2012). Need for improved treatment of postoperative pain. Dan Med J 59:A4401.

McClure JH. (1996). Ropivacaine. Br J Anaesth 76:300–7.

Ottoboni T, Quart B, Pawasauskas J, et al. (2020). Mechanism of action of HTX-011: a novel, extended-release, dual-acting local anesthetic formulation for postoperative pain. Reg Anesth Pain Med 45:117–23.

Peskin RM. (2005). Handbook of local anesthesia. N Y State Dent J 71:76–7.

Prabhakar A, Ward CT, Watson M, et al. (2019). Liposomal bupivacaine and novel local anesthetic formulations. Best Pract Res Clin Anaesthesiol 33:425–32.

Rawal N. (2016). Current issues in postoperative pain management. Eur J Anaesthesiol 33:160–71.

Safakhah HA, Taghavi T, Rashidy-Pour A, et al. (2016). Effects of saffron (*Crocus sativus* L.) stigma extract and its active constituent crocin on neuropathic pain responses in a rat model of chronic constriction injury. Iran J Pharm Res 15:253–61.

Samad TA, Moore KA, Sapirstein A, et al. (2001). Interleukin-1beta-mediated induction of Cox-2 in the CNS contributes to inflammatory pain hypersensitivity. Nature 410:471–5.

Scott DB, Lee A, Fagan D, et al. (1989). Acute toxicity of ropivacaine compared with that of bupivacaine. Anesth Analg 69:563–9.

Shah J, Votta-Velis EG, Borgeat A. (2018). New local anesthetics. Best Pract Res Clin Anaesthesiol 32:179–85.

Shah PP, Desai PR, Channer D, Singh M. (2012). Enhanced skin permeation using polyarginine modified nanostructured lipid carriers. J Control Release 161:735–45.

Viscusi E, Minkowitz H, Winkle P, et al. (2019). HTX-011 reduced pain intensity and opioid consumption versus bupivacaine HCl in herniorrhaphy: results from the phase 3 EPOCH 2 study. Hernia 23:1071–80.

Wang Y, Wang S, Shi P. (2016). Transcriptional transactivator peptide modified lidocaine-loaded nanoparticulate drug delivery system for topical anesthetic therapy. Drug Deliv 23:3193–9.

Wu CL, Raja SN. (2011). Treatment of acute postoperative pain. Lancet 377:2215–25.

Yang Y, Qiu D, Liu Y, Chao L. (2019). Topical anesthetic analgesic therapy using the combination of ropivacaine and dexmedetomidine: hyaluronic acid modified long-acting nanostructured lipid carriers containing a skin penetration enhancer. Drug Des Devel Ther 13:3307–19.

You P, Yuan R, Chen C. (2017). Design and evaluation of lidocaine- and prilocaine-coloaded nanoparticulate drug delivery systems for topical anesthetic analgesic therapy: a comparison between solid lipid nanoparticles and nanostructured lipid carriers. Drug Des Devel Ther 11:2743–52.

Yue Y, Zhao D, Yin Q. (2018). Hyaluronic acid modified nanostructured lipid carriers for transdermal bupivacaine delivery: in vitro and in vivo anesthesia evaluation. Biomed Pharmacother 98:813–20.

Zhai Y, Xu R, Wang Y, et al. (2015). Ethosomes for skin delivery of ropivacaine: preparation, characterization and ex vivo penetration properties. J Liposome Res 25:316–24.

Zhang L, Wang J, Chi H, Wang S. (2016). Local anesthetic lidocaine delivery system: chitosan and hyaluronic acid-modified layer-by-layer lipid nanoparticles. Drug Deliv 23:3529–37.

Zhang S, Li J, Hu S, et al. (2018). Triphenylphosphonium and D-α-tocopheryl polyethylene glycol 1000 succinate-modified, tanshinone IIA-loaded lipid–polymeric nanocarriers for the targeted therapy of myocardial infarction. Int J Nanomedicine 13:4045–57.

Zhang Y, Yue Y, Chang M. (2017). Local anaesthetic pain relief therapy: in vitro and in vivo evaluation of a nanotechnological formulation co-loaded with ropivacaine and dexamethasone. Biomed Pharmacother 96:443–9.